

Supporting Information

Tuning charge transfer properties in symmetric and asymmetric pyrrolo[3,2-*b*]pyrrole derivatives with hybridized local and charge-transfer characteristics

Jie Su,^a Jian Wei,^a Kaishun Ye,^a Feiyang Li,^{*a} Mengzhu Wang,^b Qiuxia Li,^a Aihua Yuan,^a Qiang Zhao,^{*b} and Chao Shi^{*a}

^a School of Environmental and Chemical Engineering, Jiangsu University of Science and Technology, Zhenjiang 212100, China. E-mail: lifeiyang@just.edu.cn, shichao@just.edu.cn.

^b State Key Laboratory of Flexible Electronics (LoFE) & Institute of Advanced Materials (IAM), Nanjing University of Posts & Telecommunications, 9 Wenyuan Road, Nanjing 210023, China. E-mail: iamqzhao@njupt.edu.cn.

Table of Contents

| | |
|---|-----------|
| 1. Experimental procedures..... | 3 |
| 1.1. Chemical reagents and materials | 3 |
| 1.2. Measurements..... | 3 |
| 1.3. Synthetic details..... | 3 |
| 2. Theoretical calculations | 6 |
| 3. Photophysical properties..... | 9 |
| 4. Crystal analysis..... | 16 |
| 5. ^1H and ^{13}C NMR spectra..... | 17 |
| 6. MS spectra..... | 22 |
| 7. References | 25 |

1. Experimental procedures

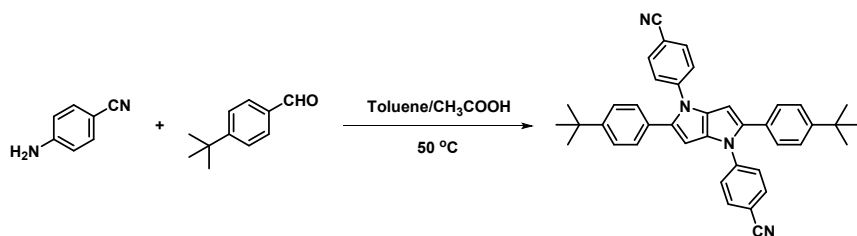
1.1. Chemical reagents and materials

All reagents were purchased from Energy Chemical and used without further purification during synthesis.

1.2. Measurements

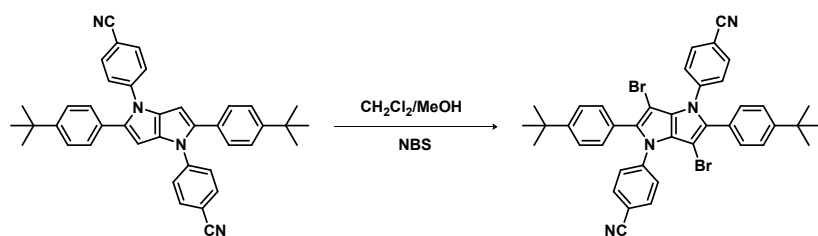
^1H NMR and ^{13}C NMR spectra were recorded on a Jeol JNM-ECZ400S/L1 NMR System Spectrometer, and the molecular weight was characterized by the Agilent Technologies 5973N (EI). The UV-vis absorption spectra were recorded on the Hitachi U-3010 UV-Visible Spectrophotometer. Photoluminescence spectra was measured on the HITACHI fluorescence spectrophotometer F-4700 and FS5. The absolute PL quantum yields of compounds were obtained on FLS980 with integrating sphere and a supplied reference plug was used as a reference sample. The radioluminescence spectra were obtained on FLS980 under irradiation of X-ray source (Mini-X2, Amptek; Au target; tube voltage, 50 kV).

1.3. Synthetic details



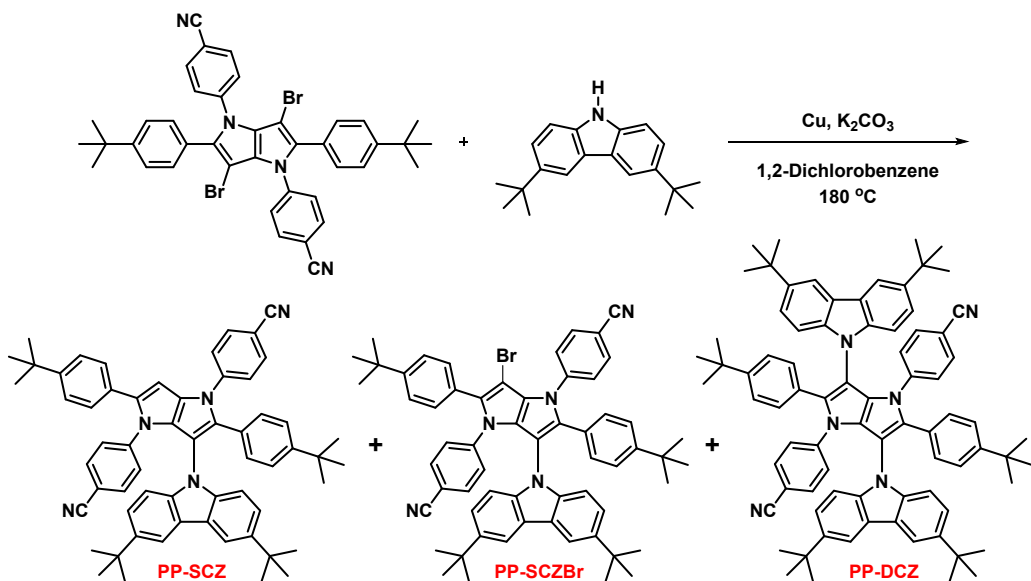
Scheme S1. The synthetic route for **PP-CN**

PP-CN: 4-Cyanoaniline (2.36 g, 20 mmol), 4-*tert*-butylbenzaldehyde (3.24 g, 20 mmol), acetic acid (10 mL) and toluene (10 mL) were added into the dry two-neck flask. The mixture was stirred at 50 °C for 1 h. Iron(III) *p*-toluenesulfonate hexahydrate (683.3 mg, 1.2 mmol) was then added, followed by the slow addition of 2,3-butanedione (860.1 mg, 10 mmol). The mixture was stirred at 50 °C overnight. The precipitate was filtered, washed with acetic acid, and dried to yield the product PP-CN (2.05 g, 35%) as a yellow solid. ^1H NMR (400 MHz, CDCl₃) δ 7.67-7.62 (m, 4H), 7.39-7.34 (m, 4H), 7.33-7.28 (m, 4H), 7.15-7.10 (m, 4H), 6.44 (s, 2H), 1.32 (s, 18H). ^{13}C NMR (100 MHz, CDCl₃) δ 150.43, 143.74, 136.17, 133.33, 130.94, 129.86, 128.07, 125.69, 125.11, 108.84, 96.86, 34.75, 31.42. EI-MS (*m/z*): 573.3 (M+1, 100 %).



Scheme S2. The synthetic route for **PP-CNBr**

PP-CNBr: Compound **PP-CN** (573 mg, 10 mmol) was dissolved in dichloromethane (20 mL) in a dry two-neck flask. A solution of *N*-bromosuccinimide in dichloromethane (356 mg in 10 mL) was added dropwise with stirring at room temperature. The reaction mixture was stirred for 15 minutes, and the reaction mixture was extracted with dichloromethane and deionized water (3×50 mL). The organic layers were combined and concentrated under reduced pressure. The crude product was purified by column chromatography, eluting with petroleum ether/dichloromethane (2:1, v/v), to afford the desired compound **PP-CNBr** (310 mg, 43%) as a white solid. ^1H NMR (400 MHz, CDCl_3) δ 7.67-7.57 (m, 4H), 7.43-7.33 (m, 4H), 7.31-7.28 (m, 4H), 7.13-7.06 (m, 4H), 1.30 (s, 18H). ^{13}C NMR (100 MHz, CDCl_3) δ 151.25, 140.76, 132.35, 130.49, 128.93, 126.83, 126.65, 125.22, 118.45, 110.76, 82.14, 34.69, 31.21. EI-MS (*m/z*): 730.1 ($M+2$, 100 %).



Scheme S3. The synthetic route for **PP-SCZ** and **PP-DCZ**

PP-SCZ/PP-DCZ: **PP-CNBr** (36.5 mg, 0.05 mmol), 3,6-di-*tert*-butylcarbazole (29.3 mg, 0.105 mmol), copper powder (20.0 mg, 0.315 mmol), and potassium carbonate (29.0 mg, 0.21 mmol) were added to a 50 mL two-neck flask. Under a nitrogen atmosphere, 10 mL of anhydrous 1,2-dichlorobenzene was added as the solvent. The reaction mixture was heated and stirred at 180 °C for 3 days. The mixture was cooled to room temperature, and the solvent was removed under reduced pressure. The crude product was purified by column chromatography with petroleum ether/dichloromethane (4:1, v/v) as the eluent to afford the target compounds **PP-SCZ** and **PP-DCZ**.

PP-SCZ: ^1H NMR (400 MHz, CDCl_3) δ 7.97 (d, $J = 1.4$ Hz, 2H), 7.69-7.67 (m, 2H), 7.45-7.43 (m, 2H), 7.20-7.16 (m, 4H), 7.03-7.98 (m, 4H), 6.93-6.91 (m, 2H), 6.88-6.86 (m, 2H), 6.66-6.64 (m, 2H), 6.54 (s, 1H),

6.43-6.41 (m, 2H), 1.43 (s, 18H), 1.25 (s, 9H), 1.13 (s, 9H). ^{13}C NMR (100 MHz, CDCl_3) δ 142.78, 140.97, 133.36, 131.89, 128.85, 127.80, 126.02, 125.57, 125.13, 123.45, 123.27, 115.85, 109.67, 95.40, 34.80, 32.16, 31.34, 31.21. EI-MS (m/z): 849.8 (M, 100 %).

PP-SCZBr: ^1H NMR (400 MHz, CDCl_3) δ 7.94-7.93 (d, $J = 1.9$ Hz, 2H), 7.71-7.69 (m, 2H), 7.57-7.56 (m, 2H), 7.23-7.18 (m, 4H), 7.09-7.02 (m, 2H), 6.99-6.97 (m, 2H), 6.89-6.84 (m, 4H), 6.57-6.55 (m, 2H), 6.32-6.30 (m, 2H), 1.42 (s, 18H), 1.26 (s, 9H), 1.11 (s, 9H). ^{13}C NMR (100 MHz, CDCl_3) δ 151.07, 150.74, 142.88, 141.39, 141.11, 140.95, 135.65, 133.92, 132.63, 131.72, 130.25, 129.32, 129.08, 127.06, 126.53, 126.45, 126.20, 125.89, 125.44, 125.30, 123.48, 123.35, 118.67, 118.36, 115.90, 110.89, 109.60, 109.32, 105.99, 82.64, 34.79, 34.75, 34.58, 32.14, 31.30, 31.16. EI-MS (m/z): 929.7 (M-2, 100 %).

PP-DCZ: ^1H NMR (400 MHz, CDCl_3) δ 8.01-8.00 (d, $J = 1.9$ Hz, 4H), 7.23-7.20 (m, 4H), 6.94 – 6.90 (m, 8H), 6.77-6.75 (m, 4H), 6.71-6.68 (m, 4H), 6.54-6.52 (m, 4H), 1.45 (s, 37H), 1.06 (s, 18H). EI-MS (m/z): 1126.6 (M-1, 100 %).

2. Theoretical calculations

Density functional theory (DFT) was used to optimize ground-state structures (S_0) under B3LYP/def2-SVP level. Vibrational frequency calculations were performed to verify the minimum nature of the optimized structures. Time-dependent density functional theory (TD-DFT) calculations were carried out to obtain the vertical excited states and optimize the lowest singlet excited state (S_1) and the lowest triplet excited state (T_1) under CAM-B3LYP/def2-SVP level based on S_0 structures. All the DFT/UDFT/TDDFT calculations were performed on Gaussian 09 package.¹ Spin-orbit coupling matrix elements (SOC) between singlet and triplet states were calculated by ORCA 6.0.1.^{2,3} Analysis and visualization of hole-electron distribution were finished by Multiwfn 3.8(dev) and VMD.⁴⁻⁶

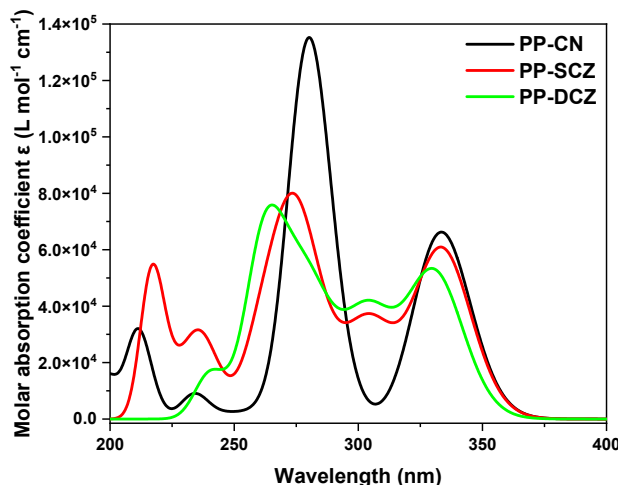


Fig. S1 The simulated UV-Vis absorption spectra of PP-CN, PP-SCZ and PP-DCZ.

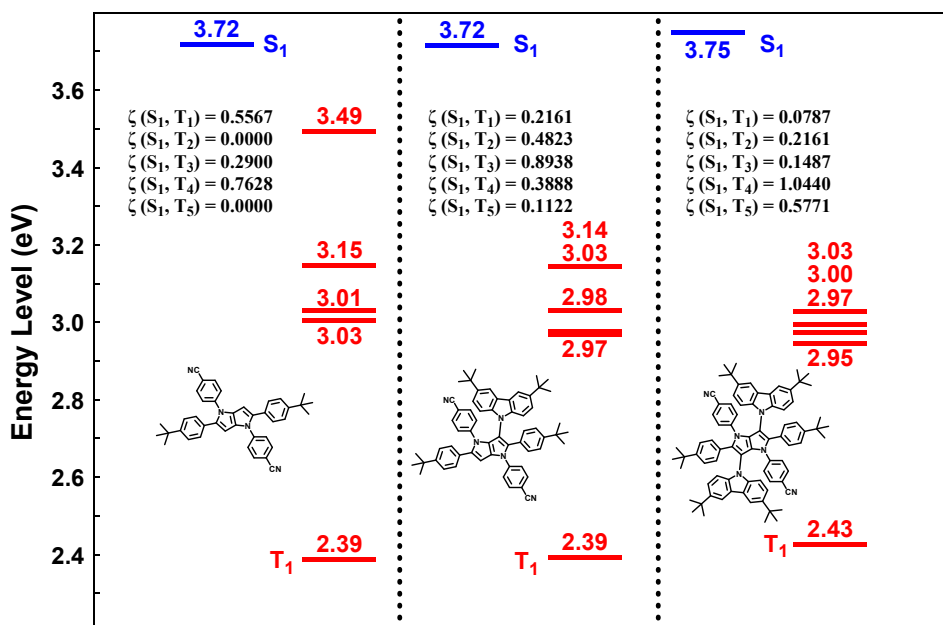


Fig. S2 The simulated energy (eV) of the vertical excited states based on the optimized S_0 structures of PP-CN, PP-SCZ and PP-DCZ, and the SOC (cm^{-1}) between the singlet and triplet states.

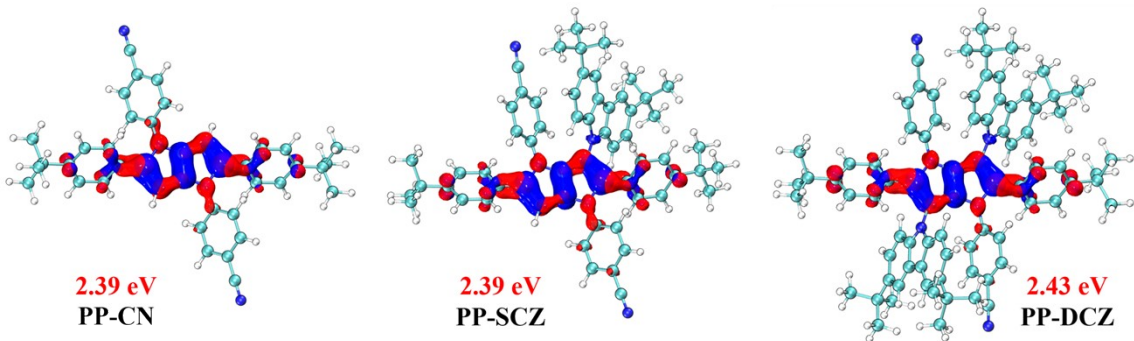


Fig. S3 The hole-electron distributions of $S_0 \rightarrow T_1$ excitation of **PP-CN**, **PP-SCZ** and **PP-DCZ**.

The interfragment charge transfer (IFCT) method was employed using the Multiwfn software to analyze charge transfer between fragments and within the fragments. The following lists the fragment regions and their corresponding charge transfer ratios. The intrinsic CT percentages in **PP-CN**, **PP-SCZ**, and **PP-DCZ** are 13.8%, 18.5%, and 19.7%, respectively.

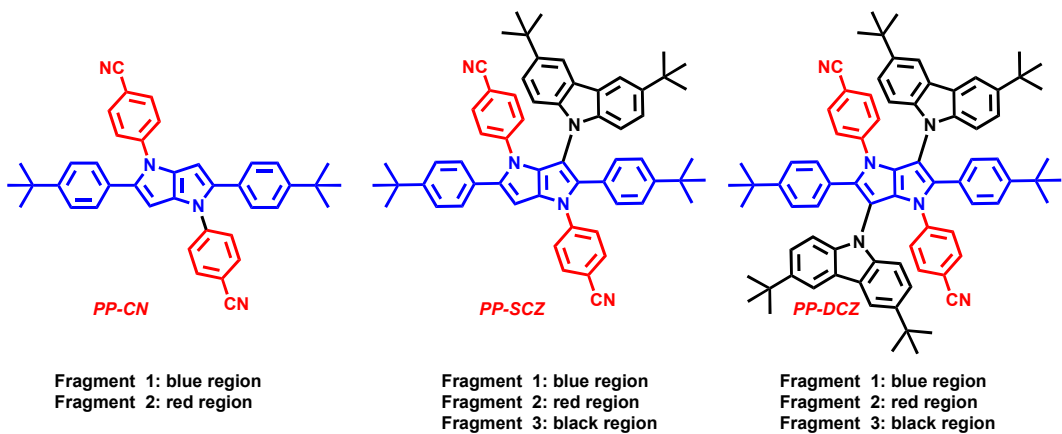


Fig. S4 The different fragment regions in hole-electron analysis of $S_0 \rightarrow S_1$ excitation of **PP-CN**, **PP-SCZ** and **PP-DCZ**.

Transferred electrons between fragments in **PP-CN**:

$$1 \rightarrow 2: 0.13098 \quad 1 < 2: 0.00663 \quad \text{Net } 1 \rightarrow 2: 0.12435$$

Intrinsic charge transfer percentage, CT(%): 13.761 %

Intrinsic local excitation percentage, LE(%): 86.239 %

Transferred electrons between fragments in **PP-SCZ**:

$$1 \rightarrow 2: 0.12385 \quad 1 < 2: 0.00534 \quad \text{Net } 1 \rightarrow 2: 0.11851$$

$$1 \rightarrow 3: 0.01312 \quad 1 < 3: 0.03695 \quad \text{Net } 1 \rightarrow 3: -0.02383$$

$$2 \rightarrow 3: 0.00009 \quad 2 < 3: 0.00562 \quad \text{Net } 2 \rightarrow 3: -0.00554$$

Intrinsic charge transfer percentage, CT(%): 18.497 %

Intrinsic local excitation percentage, LE(%): 81.503 %

Transferred electrons between fragments in **PP-DCZ**:

1 -> 2: 0.10973 1 <- 2: 0.00490 Net 1 -> 2: 0.10483

1 -> 3: 0.02254 1 <- 3: 0.05281 Net 1 -> 3: -0.03027

2 -> 3: 0.00014 2 <- 3: 0.00724 Net 2 -> 3: -0.00710

Intrinsic charge transfer percentage, CT(%): 19.737 %

Intrinsic local excitation percentage, LE(%): 80.263 %

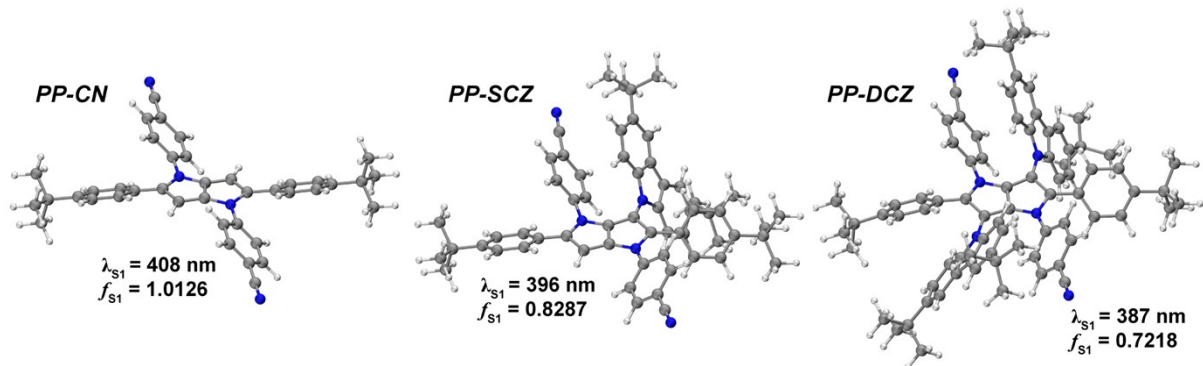


Fig. S5 The simulated emission wavelength and oscillator strength of the optimized S_1 structures of **PP-CN**, **PP-SCZ** and **PP-DCZ** under the CAM-B3LYP/def2-SVP level.

3. Photophysical properties

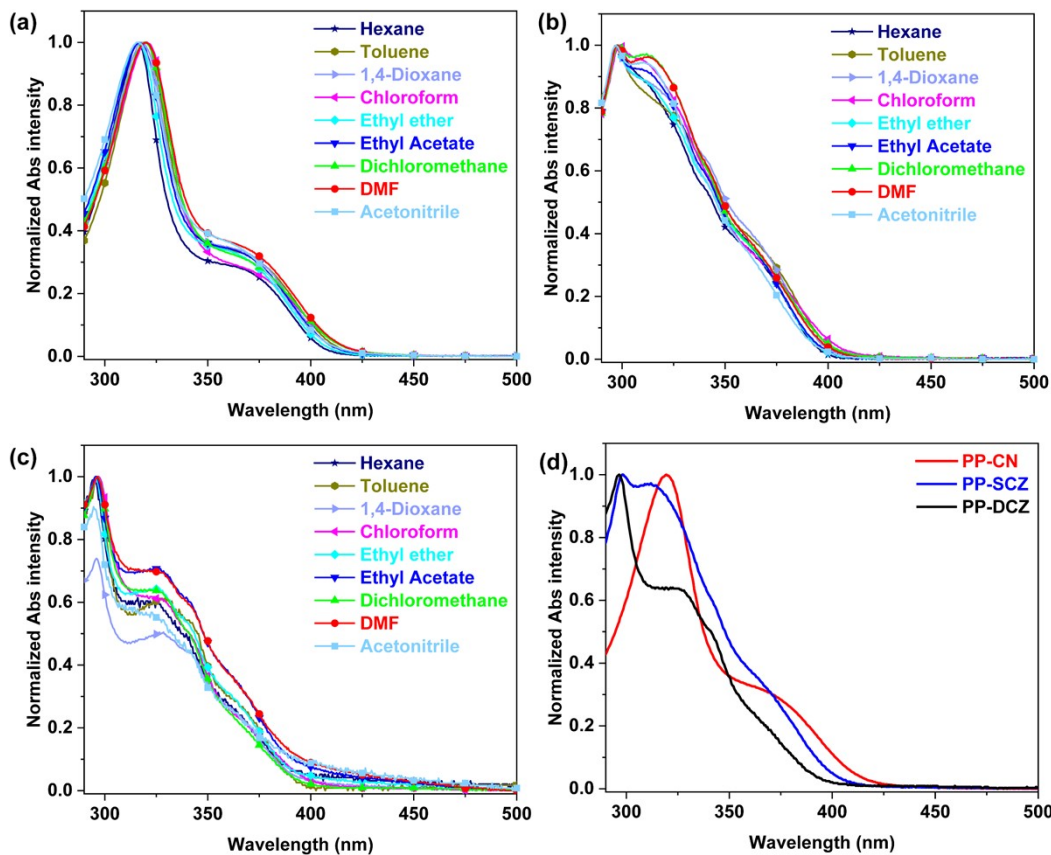


Fig. S6 Normalized absorption spectra (1.0×10^{-5} mol/L) of (a) PP-CN, (b) PP-SCZ and (c) PP-DCZ in *n*-hexane, toluene, 1,4-dioxane, chloroform, ethyl ether, ethyl acetate, dichloromethane, *N,N*-Dimethylformamide (DMF) and acetonitrile. (d) Normalized absorption spectra of PP-CN, PP-SCZ and PP-DCZ in the dichloromethane.

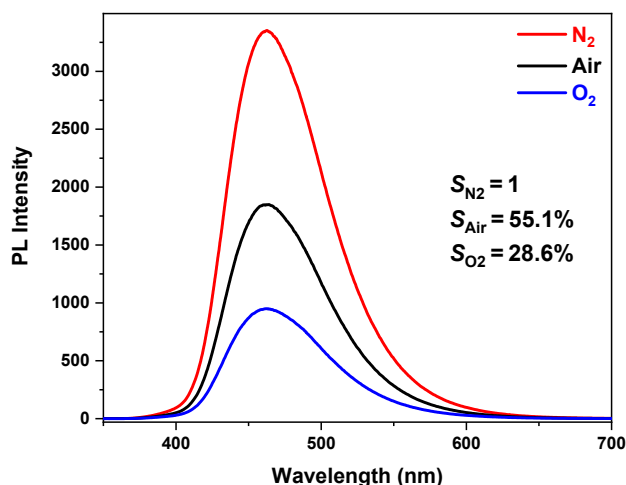


Fig. S7 PL spectra of PP-CN in the toluene under nitrogen atmosphere (red line), air atmosphere (black line) and oxygen atmosphere (blue line). The numbers inserted represent the ratio of the emission peak area under different atmosphere. ($\lambda_{ex} = 300$ nm)

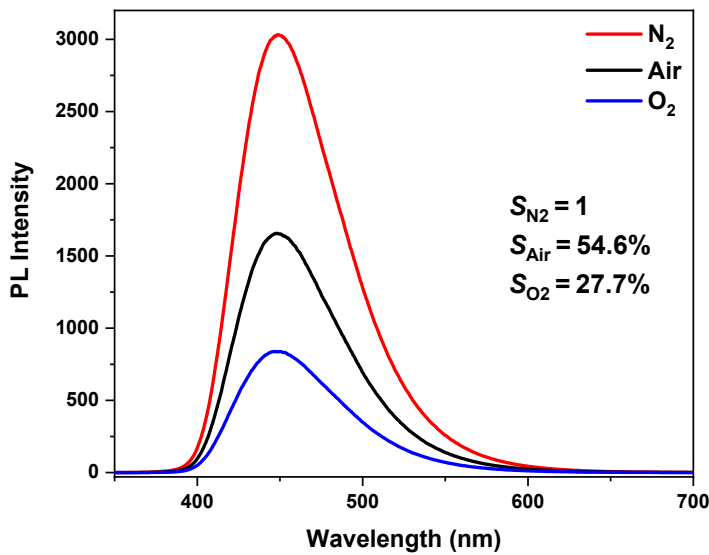


Fig. S8 PL spectra of PP-SCZ in the toluene under nitrogen atmosphere (red line), air atmosphere (black line) and oxygen atmosphere (blue line). The numbers inserted represent the ratio of the emission peak area under different atmosphere. ($\lambda_{ex} = 300$ nm)

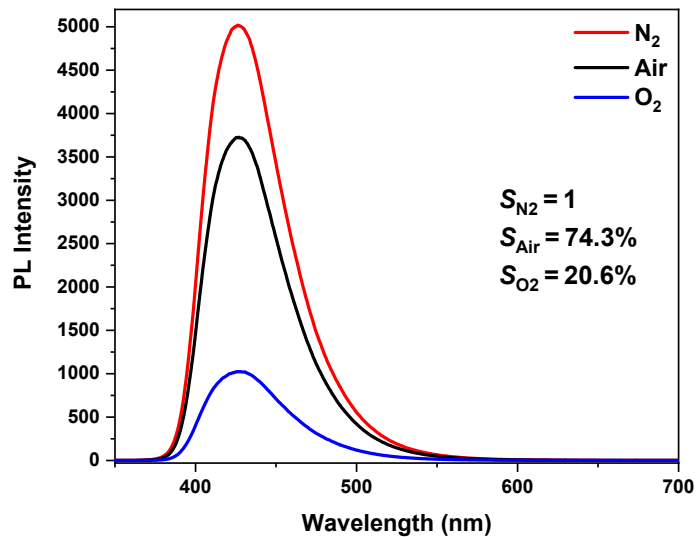


Fig. S9 PL spectra of PP-DCZ in the toluene under nitrogen atmosphere (red line), air atmosphere (black line) and oxygen atmosphere (blue line). The numbers inserted represent the ratio of the emission peak area under different atmosphere. ($\lambda_{ex} = 300$ nm)

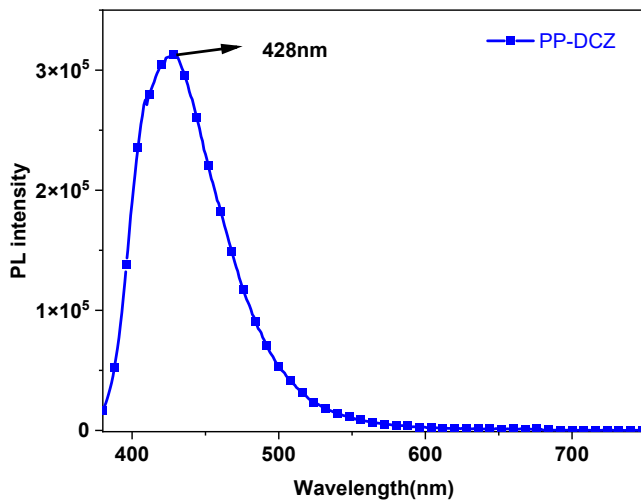


Fig. S10 PL spectra of PP-DCZ in the toluene under ambient atmosphere. ($\lambda_{\text{ex}} = 365$ nm)

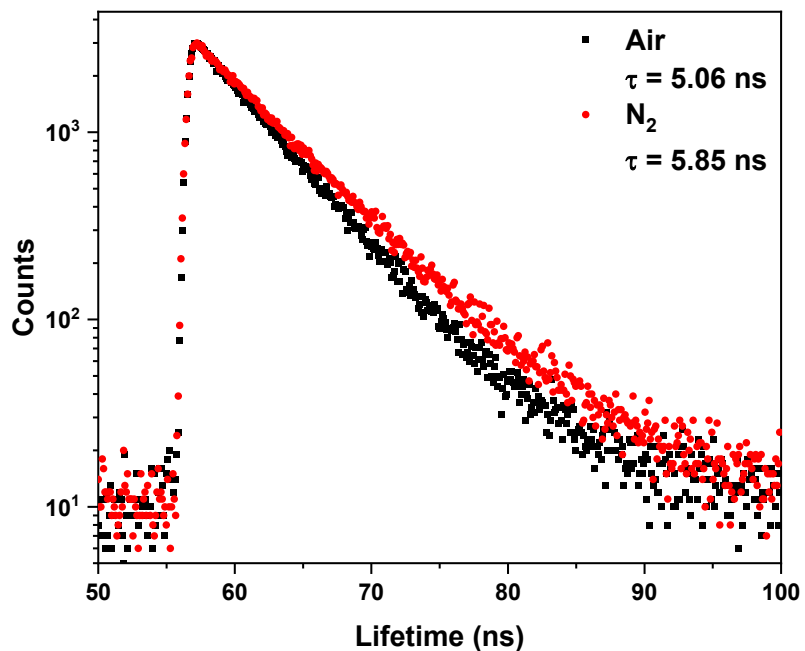


Fig. S11 Time decay profiles of PP-CN in the toluene under nitrogen atmosphere (black) and air atmosphere (red). ($\lambda_{\text{em}} = 463$ nm)

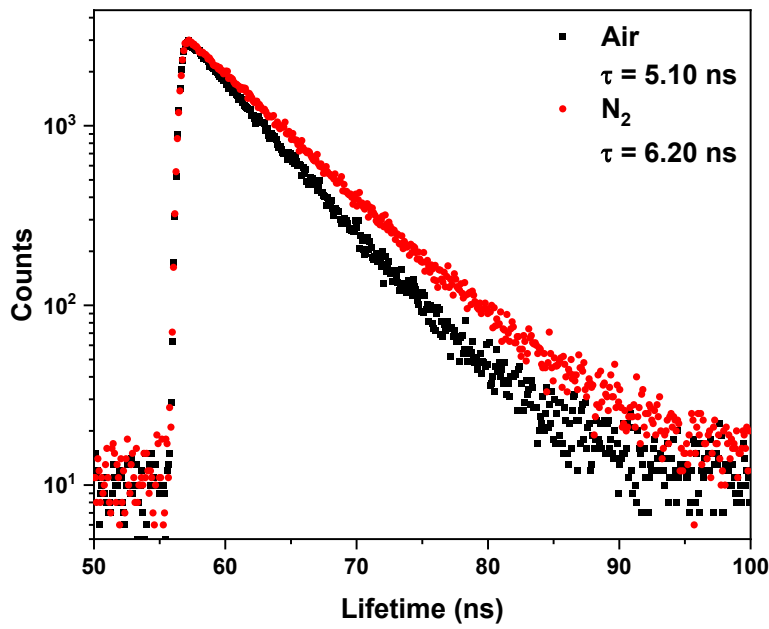


Fig. S12 Time decay profiles of PP-SCZ in the toluene under nitrogen atmosphere (black) and air atmosphere (red). ($\lambda_{\text{em}} = 447 \text{ nm}$)

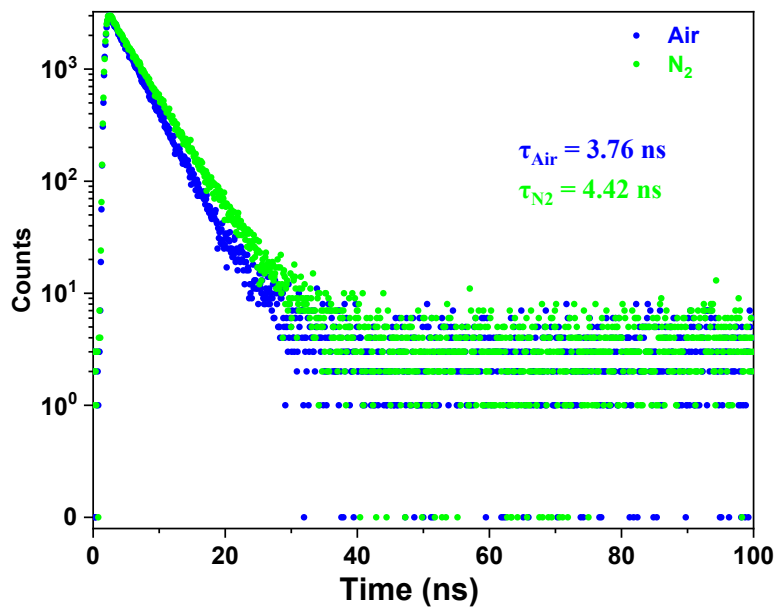


Fig. S13 Time decay profiles of PP-DCZ in the toluene under nitrogen atmosphere (green) and air atmosphere (blue). ($\lambda_{\text{em}} = 428 \text{ nm}$)

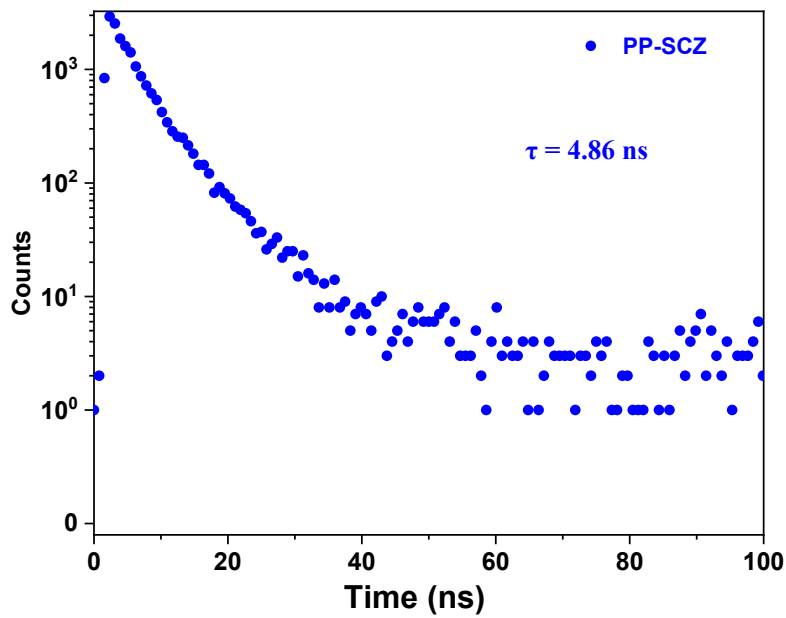


Fig. S14 Time decay profile of **PP-SCZ** in the PS film. ($\lambda_{\text{em}} = 443 \text{ nm}$)

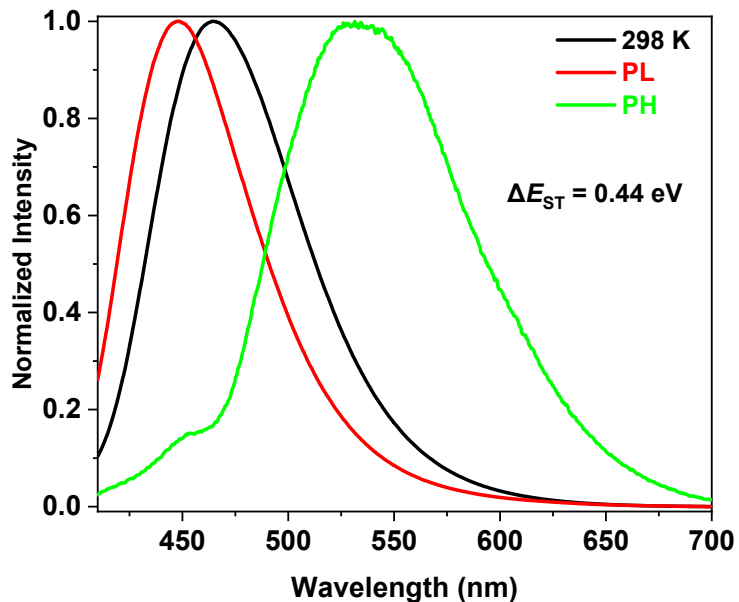


Fig. S15 Normalized photoluminescence spectra ($\lambda_{\text{ex}} = 370 \text{ nm}$) of **PP-CN** in toluene at 298 K (black line) and at 77 K (red line), and the phosphorescence spectra (green line) at 77 K.

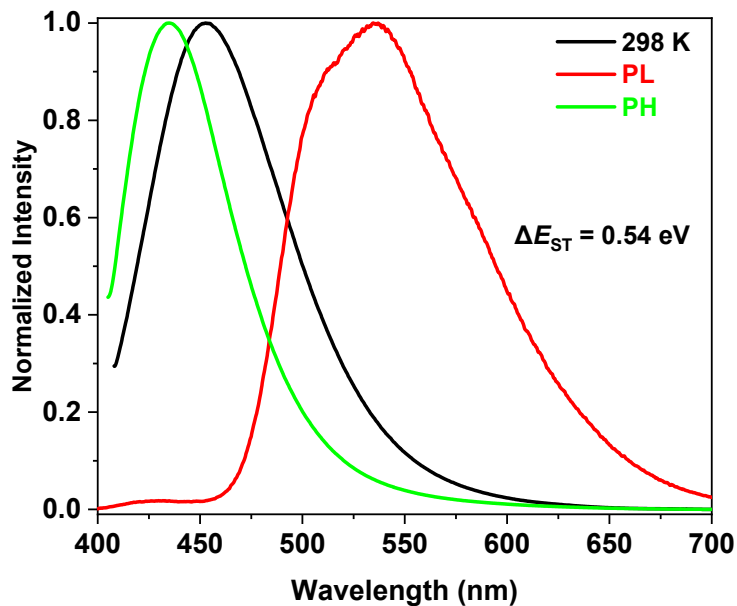


Fig. S16 Normalized photoluminescence spectra ($\lambda_{\text{ex}} = 370$ nm) of **PP-SCZ** in toluene at 298 K (black line) and at 77 K (red line), and the phosphorescence spectra (green line) at 77 K.

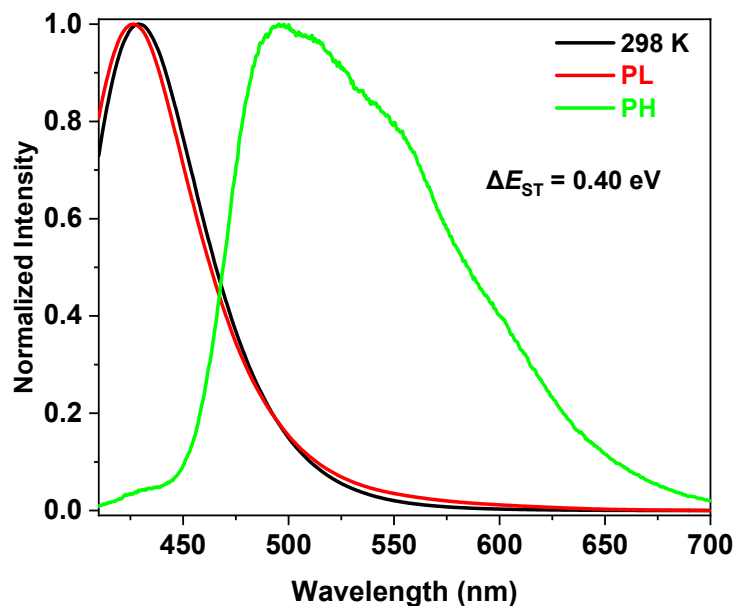


Fig. S17 Normalized photoluminescence spectra ($\lambda_{\text{ex}} = 370$ nm) of **PP-DCZ** in toluene at 298 K (black line) and at 77 K (red line), and the phosphorescence spectra (green line) at 77 K.

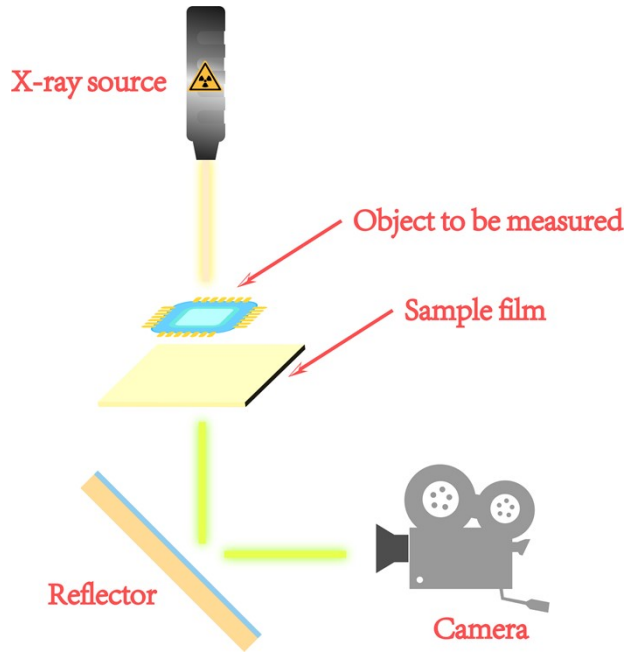


Fig. S18 The schematic illustration of X-ray imaging optical system.

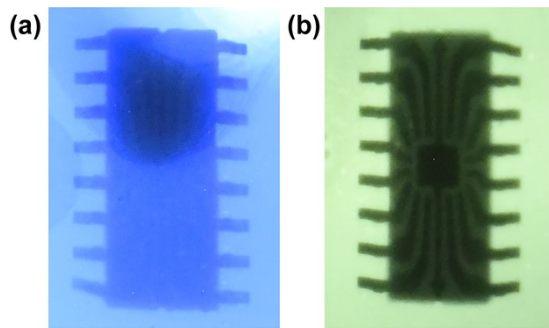


Fig. S19 The X-ray imaging of the chip using the (a) PP-SCZ-based and (b) copper cluster-based scintillation screen.

4. Crystal analysis

Single crystals of PP-SCZ were grown from mixed solutions of dichloromethane and ethanol by the solvent diffusion method. During the crystal growth process, PP-SCZBr was mixed, and the final crystal contained approximately 92% of PP-SCZ. CCDC 2415312 contains the supplementary crystallographic data for this paper. **Table S1** lists the crystallographic data for PP-SCZ.

Table S1 Crystallographic data for PP-SCZ

| Identification code | PP-SCZ |
|---|---|
| Empirical formula | C ₁₂₀ H _{117.84} Br _{0.16} N ₁₀ |
| Formula weight | 1712.86 |
| Temperature/K | 223 |
| Crystal system | triclinic |
| Space group | P-1 |
| a/Å | 8.9922(4) |
| b/Å | 10.9314(4) |
| c/Å | 28.0249(9) |
| $\alpha/^\circ$ | 81.537(2) |
| $\beta/^\circ$ | 84.208(3) |
| $\gamma/^\circ$ | 88.326(3) |
| Volume/Å ³ | 2710.58(18) |
| Z | 1 |
| $\rho_{\text{calc}}/\text{g/cm}^3$ | 1.049 |
| μ/mm^{-1} | 0.534 |
| F(000) | 913 |
| Radiation | CuK α ($\lambda = 1.54178$) |
| 2 Θ range for data collection/° | 8.178 to 137.17 |
| Index ranges | -10 ≤ h ≤ 10, -13 ≤ k ≤ 13, -33 ≤ l ≤ 33 |
| Reflections collected | 34081 |
| Independent reflections | 9925 [R _{int} = 0.0817, R _{sigma} = 0.0693] |
| Data/restraints/parameters | 9925/36/640 |
| Goodness-of-fit on F ² | 1.012 |
| Final R indexes [I>=2σ (I)] | R ₁ = 0.0563, wR ₂ = 0.1453 |
| Final R indexes [all data] | R ₁ = 0.0932, wR ₂ = 0.1702 |
| Largest diff. peak/hole / e Å ⁻³ | 0.21/-0.19 |

5. ^1H and ^{13}C NMR spectra

^1H and ^{13}C NMR spectra were recorded with CDCl_3 as the solvents and tetramethylsilane (TMS) as the internal standard (^1H NMR: TMS at 0.00 ppm).

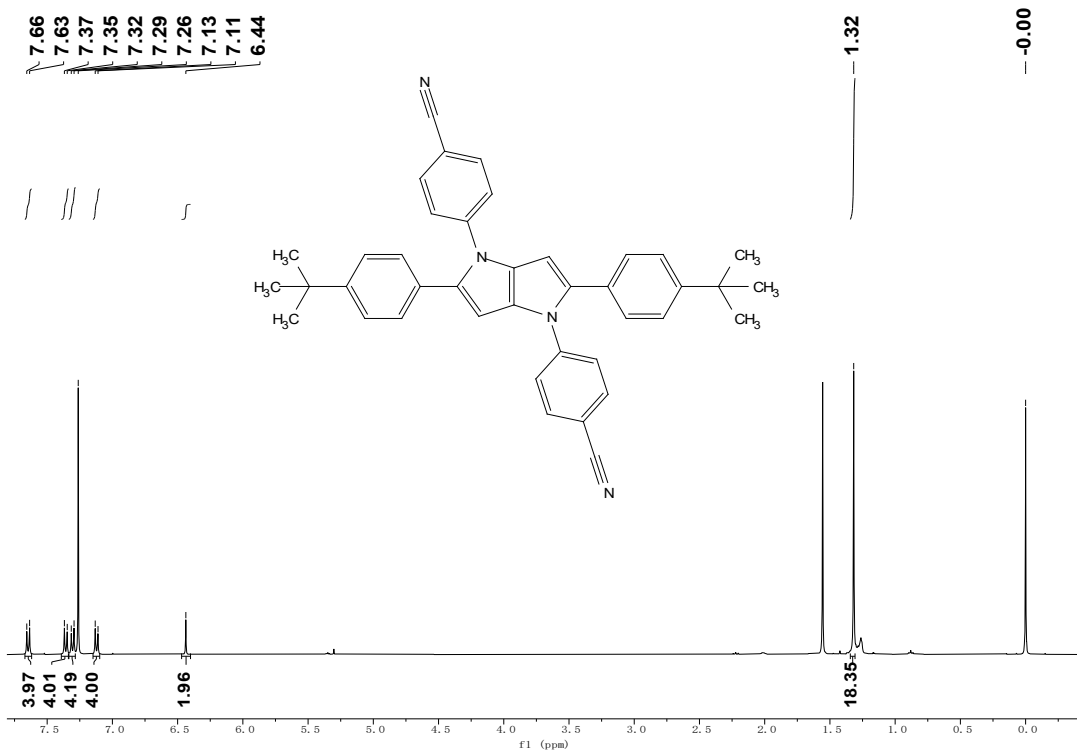


Fig. S20 The ^1H NMR spectra of PP-CN.

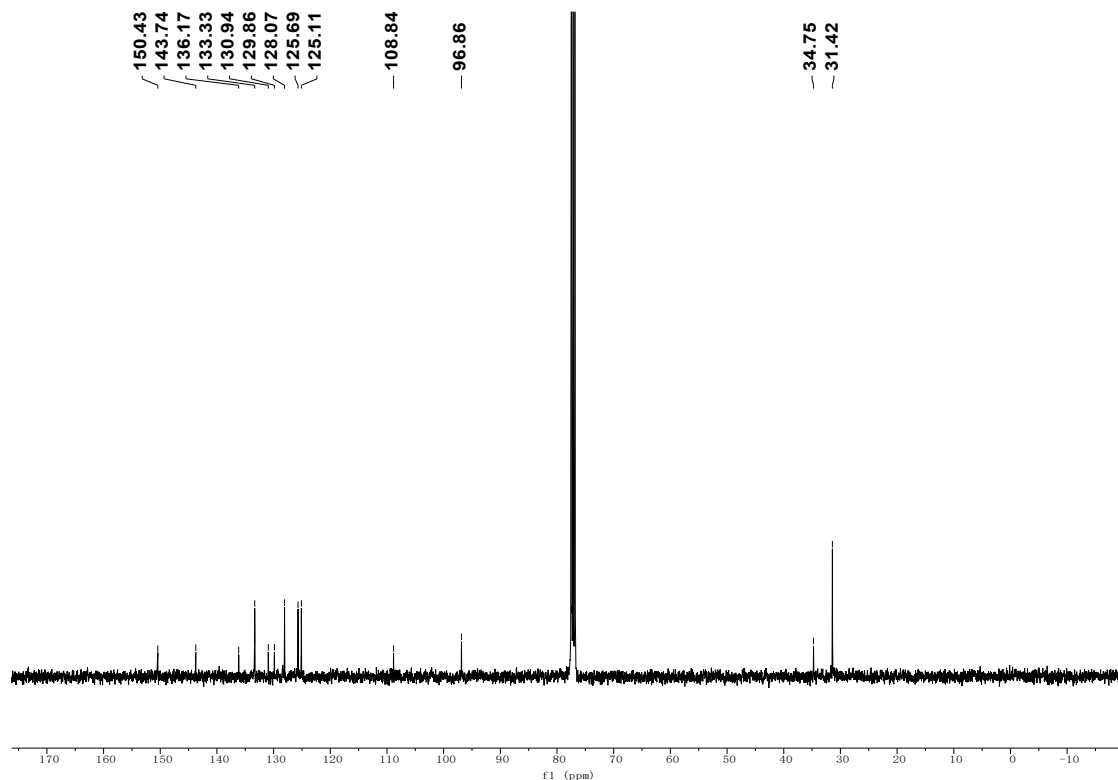


Fig. S21 The ^{13}C NMR spectra of PP-CN.

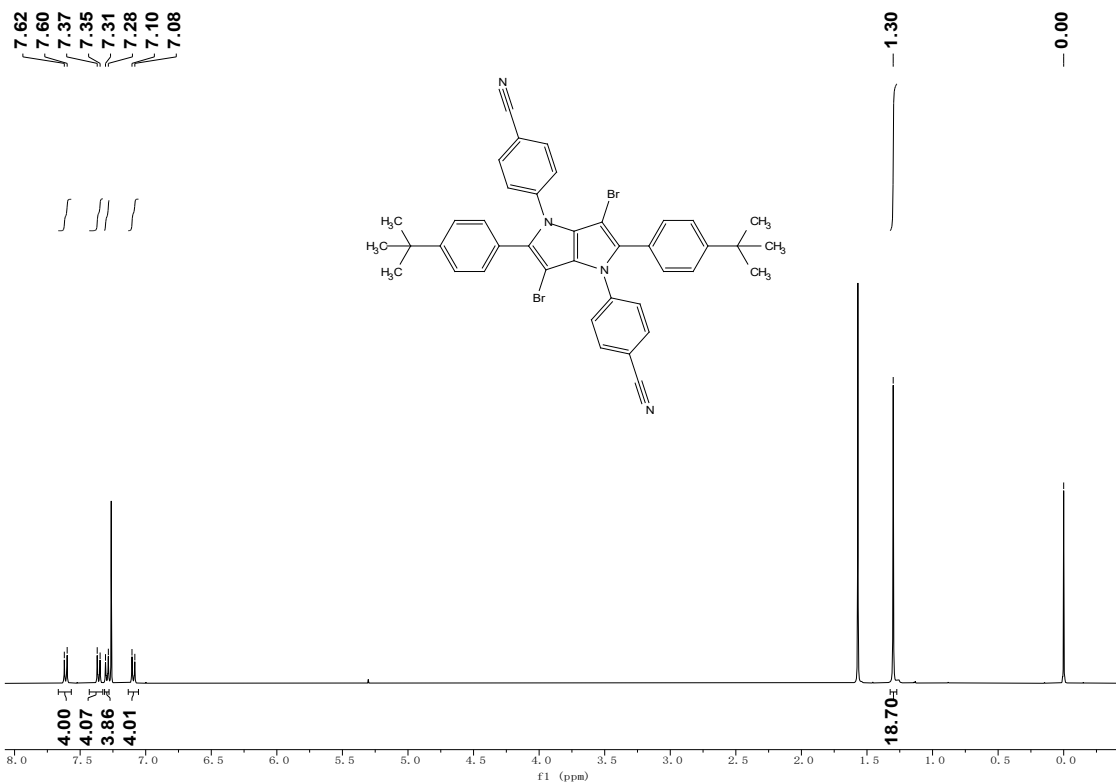


Fig. S22 The ^1H NMR spectra of PP-CNBr.

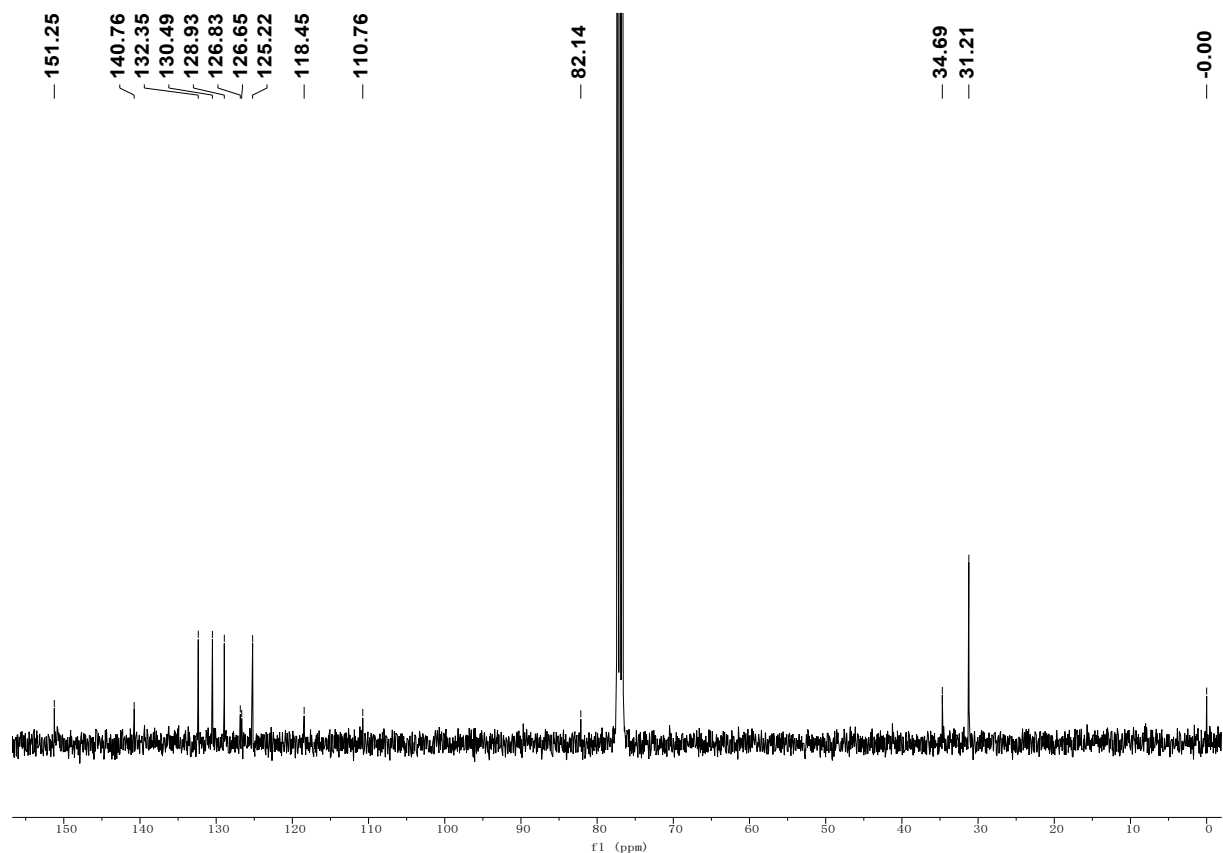


Fig. S23 The ^{13}C NMR spectra of PP-CNBr.

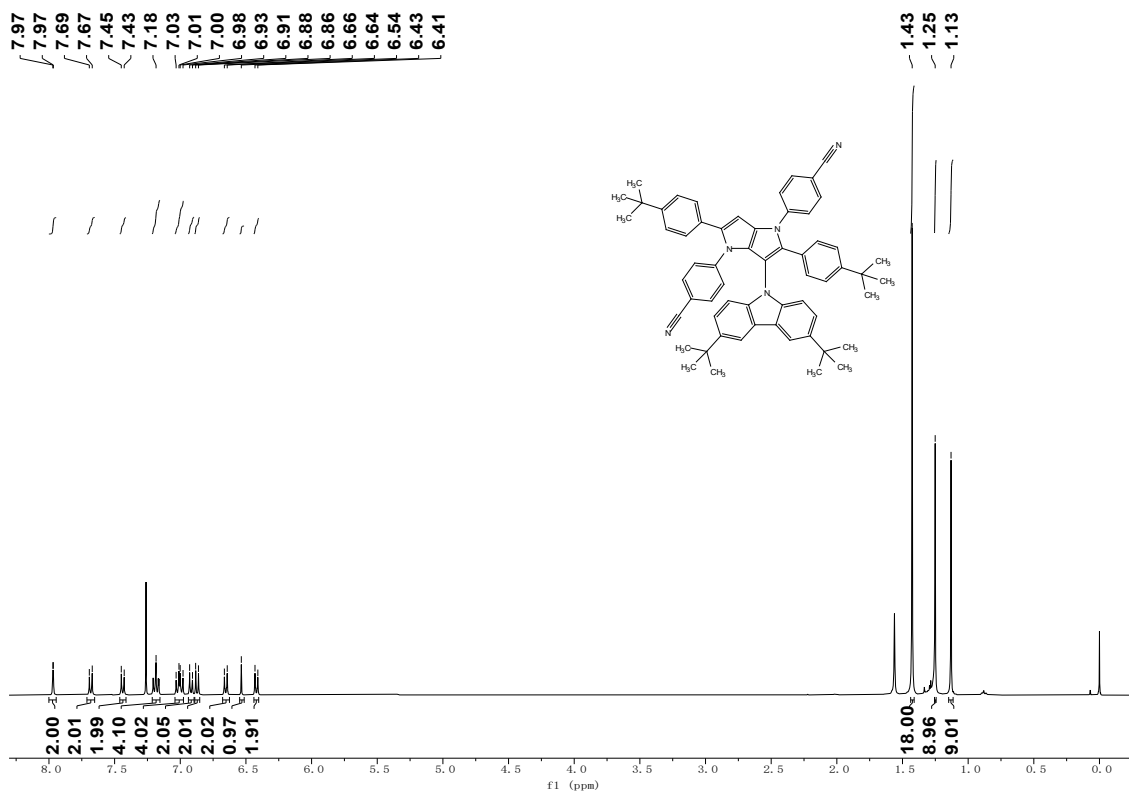


Fig. S24 The ¹H NMR spectra of PP-SCZ.

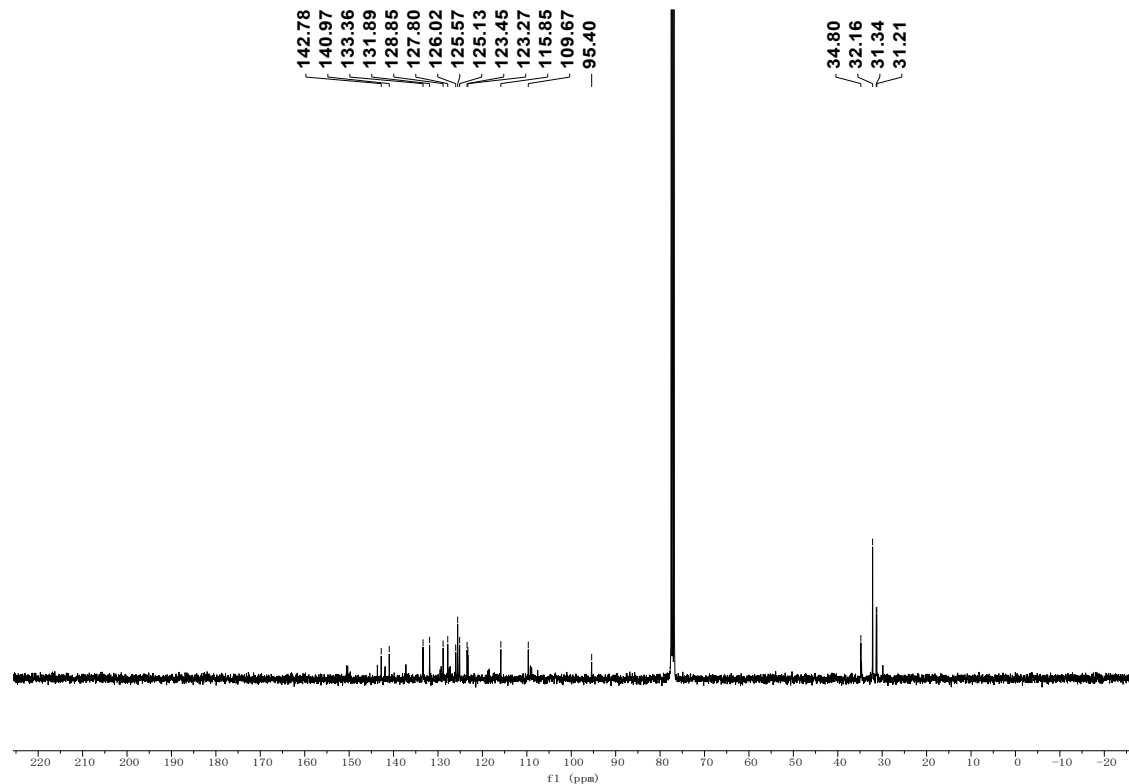


Fig. S25 The ¹³C NMR spectra of PP-SCZ.

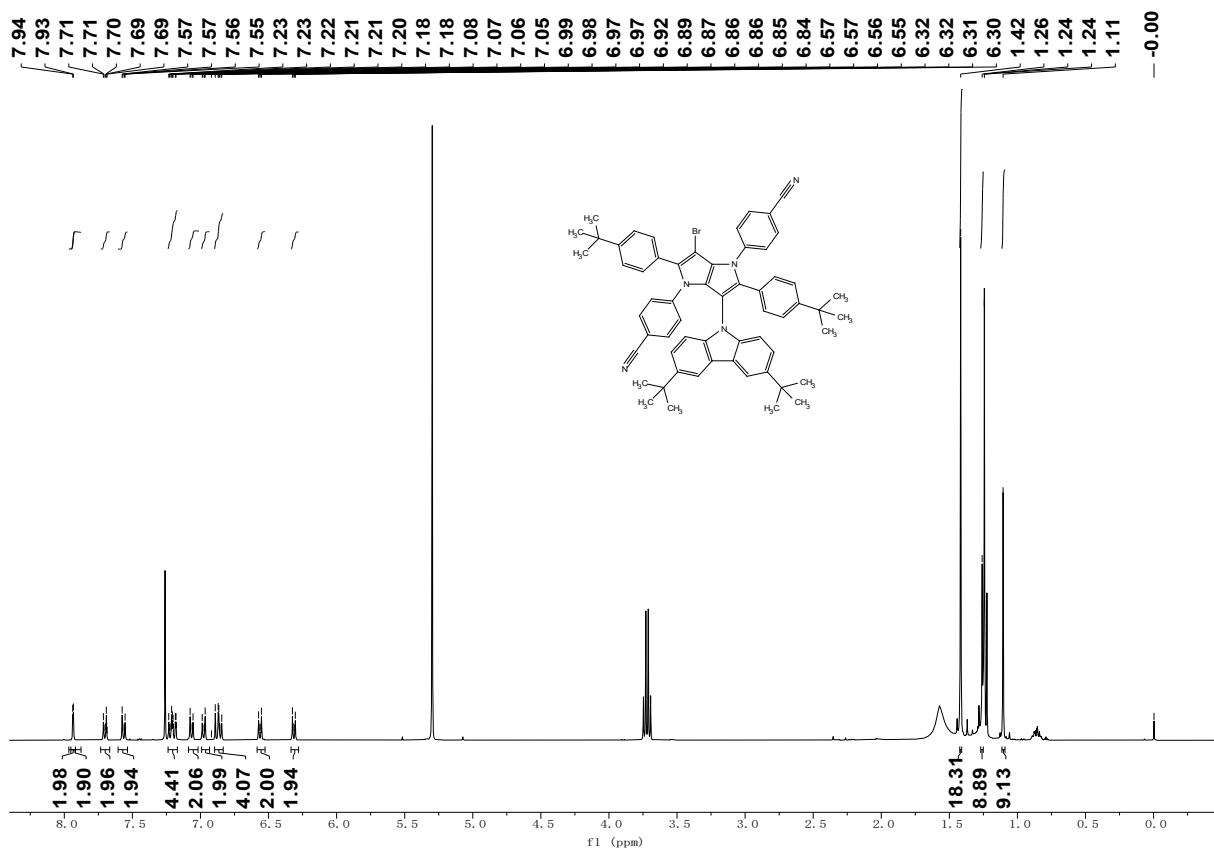


Fig. S26 The ¹H NMR spectra of PP-SCZBr.

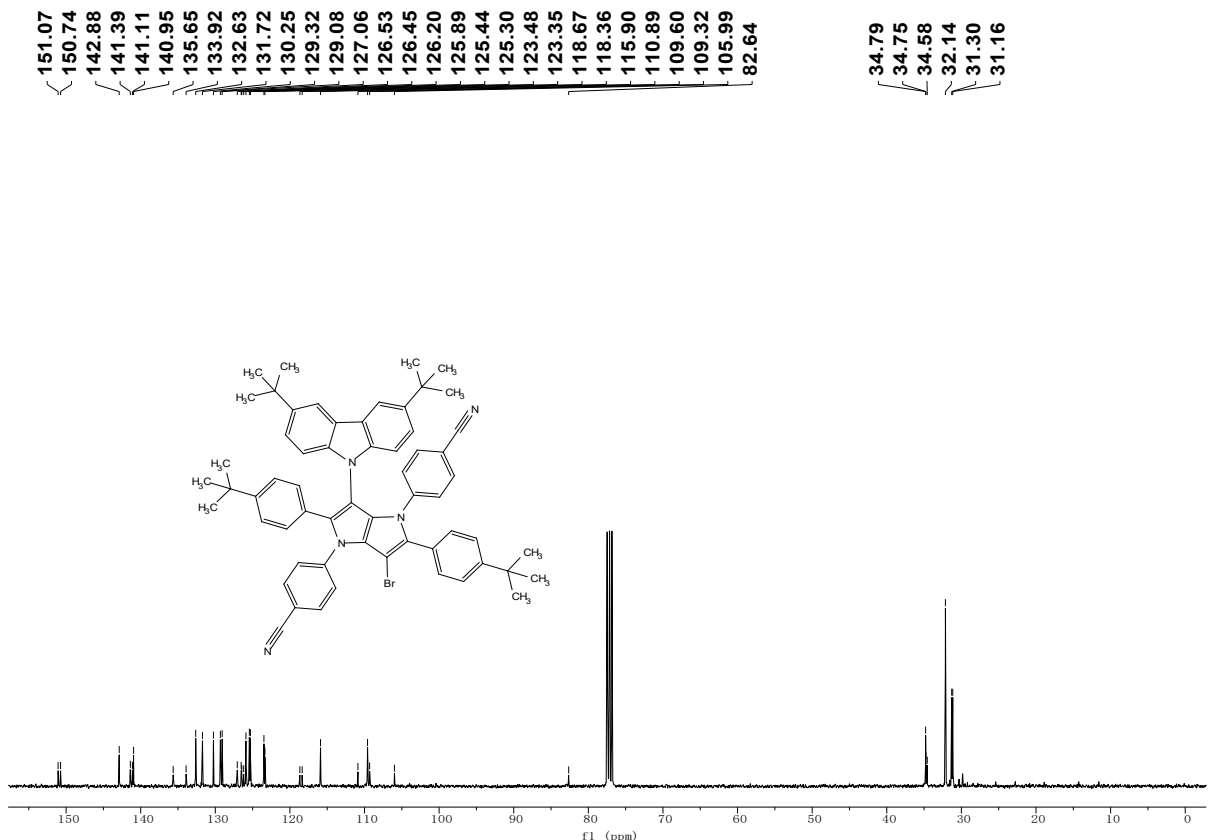


Fig. S27 The ¹³C NMR spectra of PP-SCZBr.

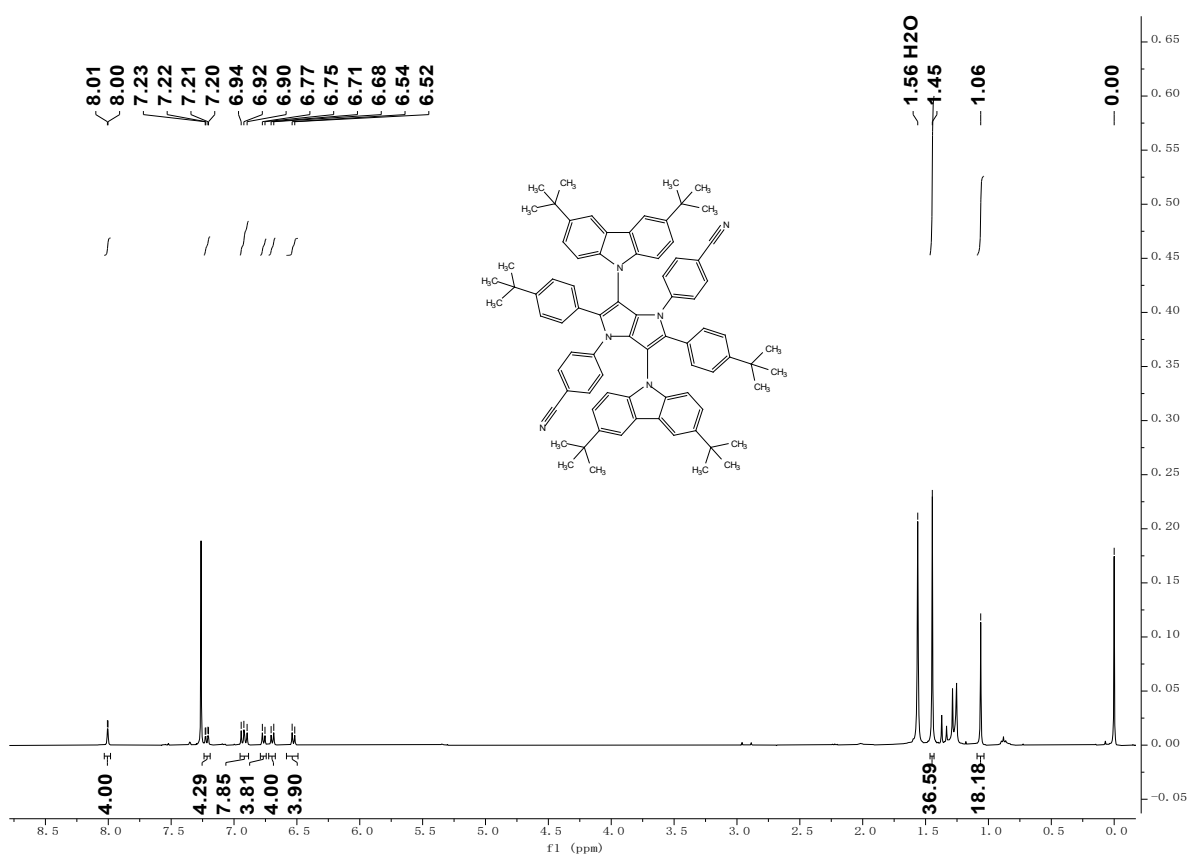


Fig. S28 The ^1H NMR spectra of PP-DCZ.

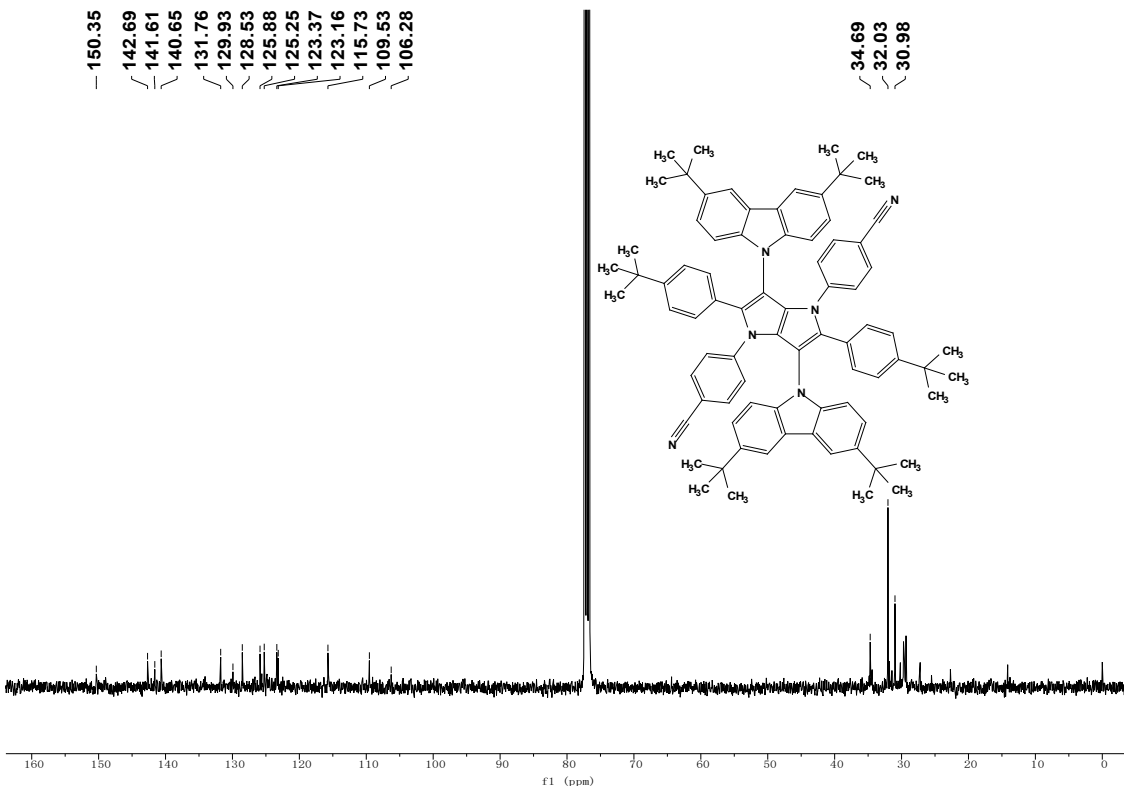


Fig. S29 The ^{13}C NMR spectra of PP-DCZ.

6. MS spectra

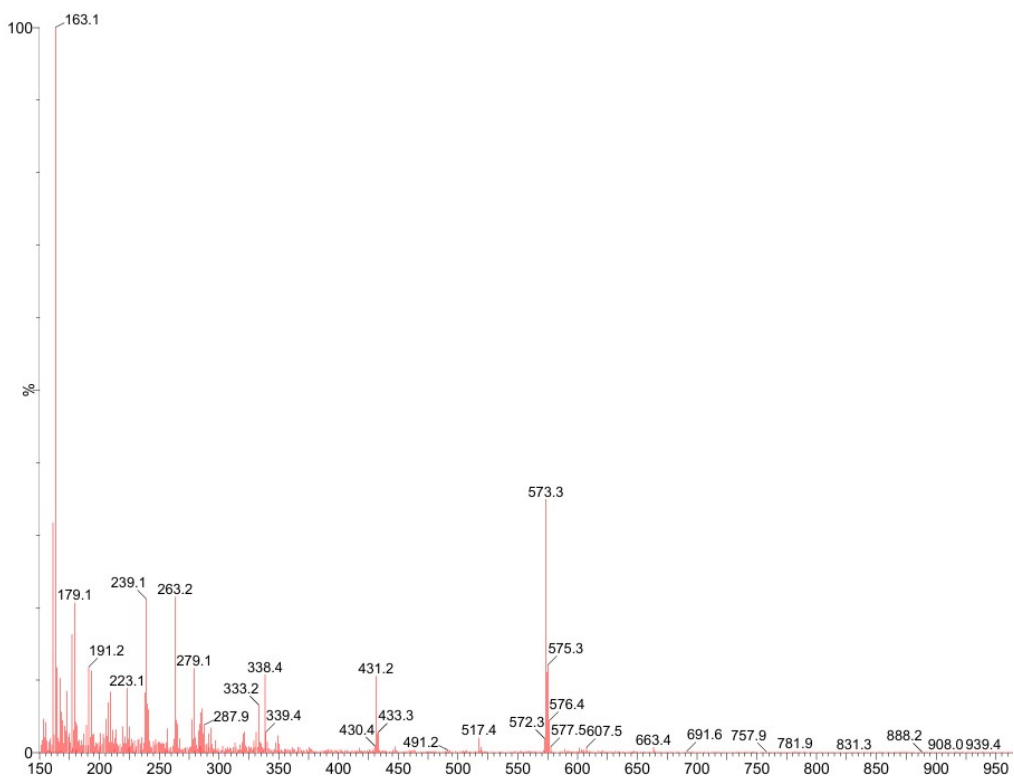


Fig. S30 MS spectra of PP-CN.

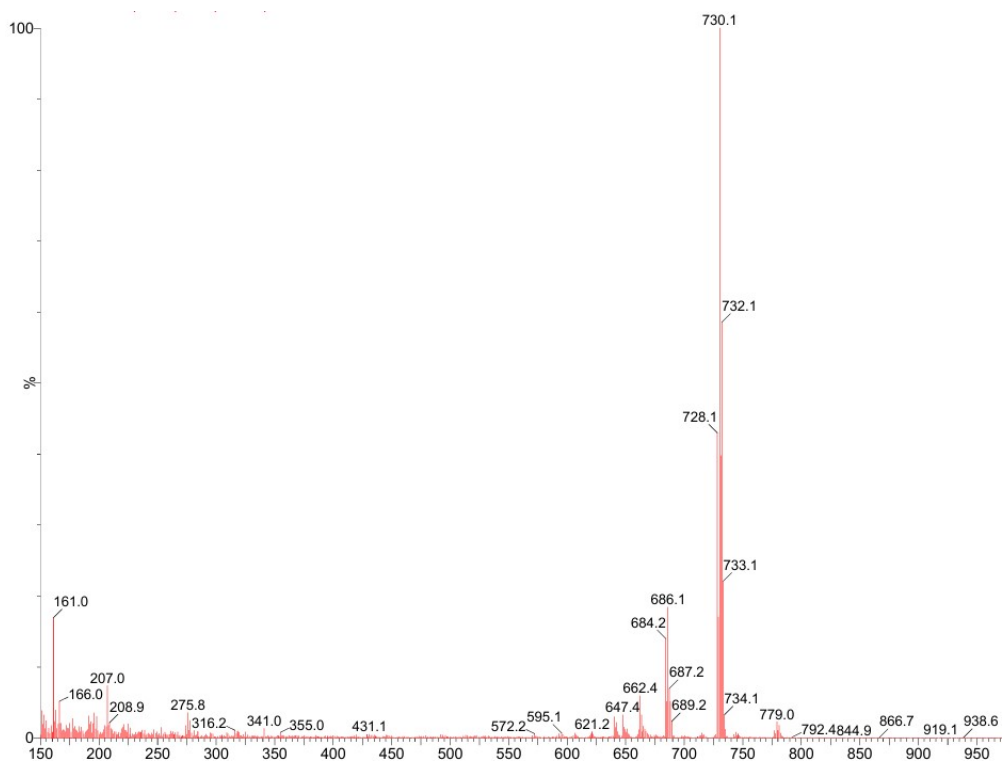


Fig. S31 MS spectra of PP-CNBr.

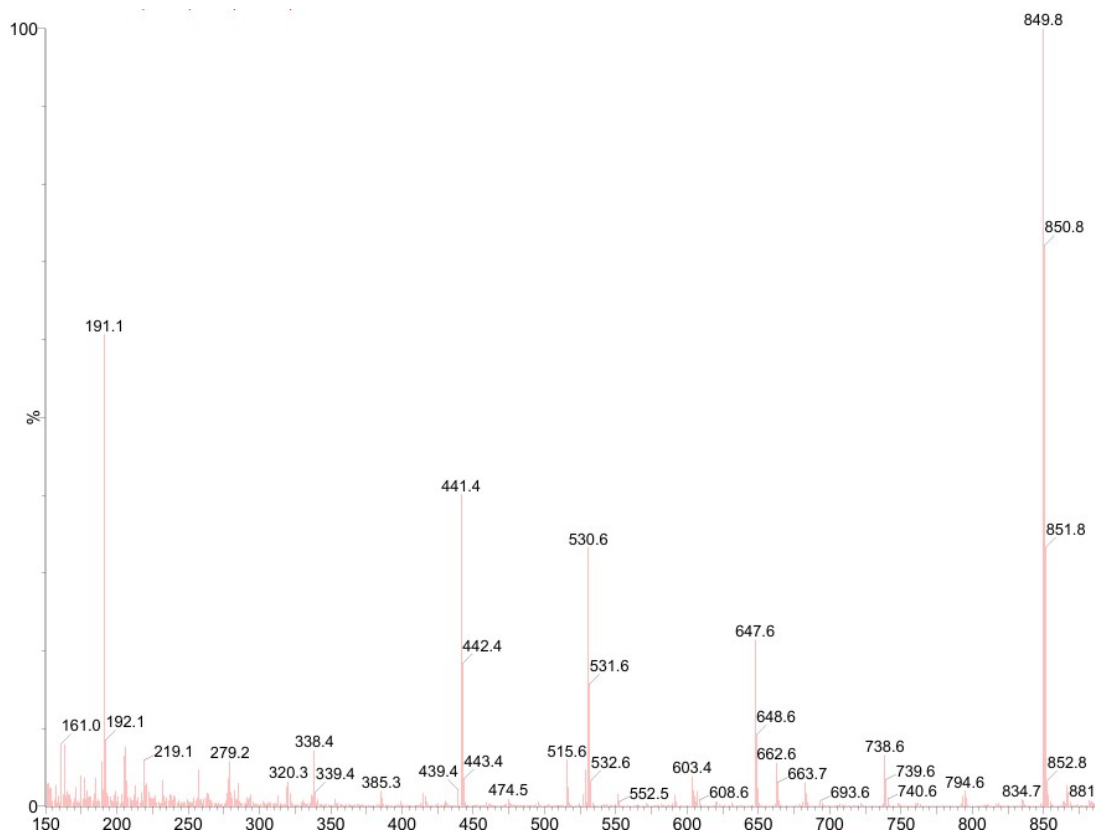


Fig. S32 MS spectra of PP-SCZ.

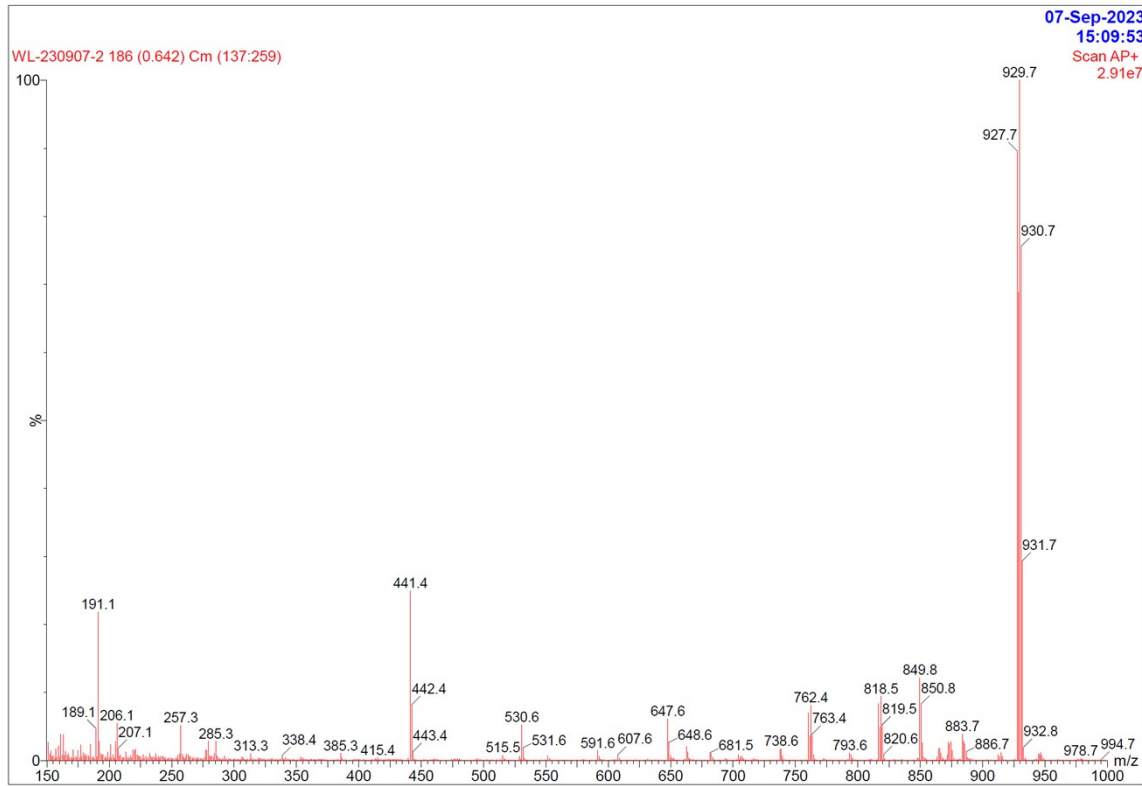


Fig. S33 MS spectra of PP-SCZBr.

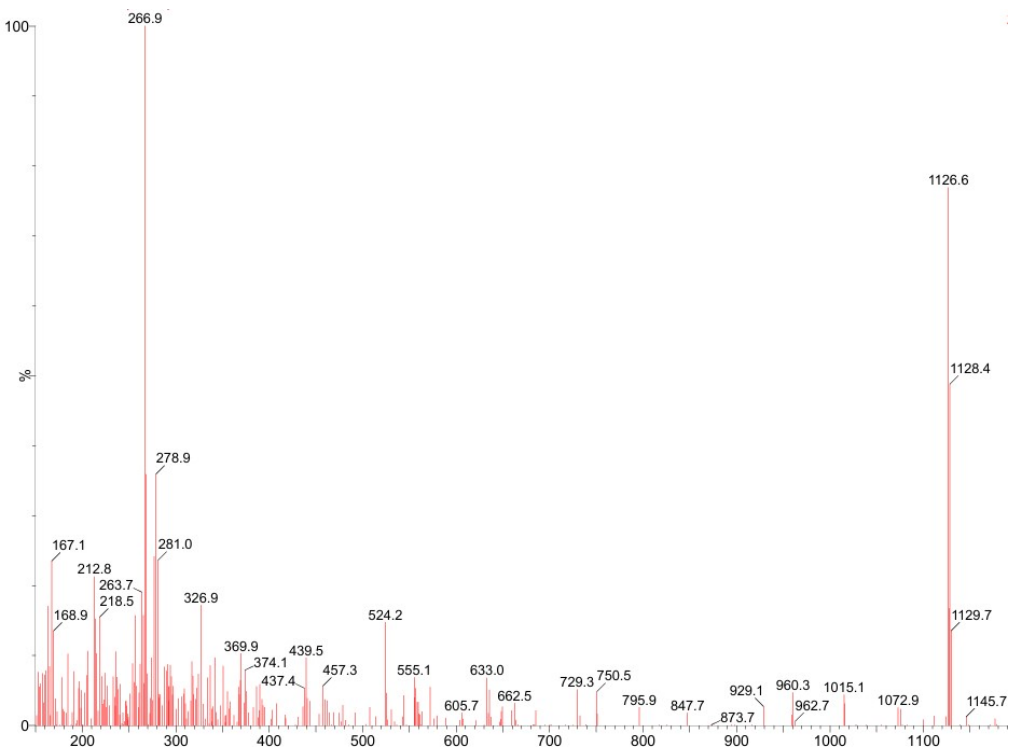


Fig. S34 MS spectra of PP-DCZ.

7. References

1. M. J. Frisch, G. W. Trucks, H. B. Schlegel, G. E. Scuseria, M. A. Robb, J. R. Cheeseman, G. Scalmani, V. Barone, B. Mennucci, G. A. Petersson, H. Nakatsuji, M. Caricato, X. Li, H. P. Hratchian, A. F. Izmaylov, J. Bloino, G. Zheng, J. L. Sonnenberg, M. Hada, M. Ehara, K. Toyota, R. Fukuda, J. Hasegawa, M. Ishida, T. Nakajima, Y. Honda, O. Kitao, H. Nakai, T. Vreven, J. A. Montgomery, Jr., J. E. Peralta, F. Ogliaro, M. Bearpark, J. J. Heyd, E. Brothers, K. N. Kudin, V. N. Staroverov, R. Kobayashi, J. Normand, K. Raghavachari, A. Rendell, J. C. Burant, S. S. Iyengar, J. Tomasi, M. Cossi, N. Rega, J. M. Millam, M. Klene, J. E. Knox, J. B. Cross, V. Bakken, C. Adamo, J. Jaramillo, R. Gomperts, R. E. Stratmann, O. Yazyev, A. J. Austin, R. Cammi, C. Pomelli, J. W. Ochterski, R. L. Martin, K. Morokuma, V. G. Zakrzewski, G. A. Voth, P. Salvador, J. J. Dannenberg, S. Dapprich, A. D. Daniels, Ö. Farkas, J. B. Foresman, J. V. Ortiz, J. Cioslowski, and D. J. Fox, *Gaussian 09* (Gaussian, Inc., Wallingford CT, 2009).
2. F. Neese, *Wires Comput. Mol. Sci.*, 2012, **2**, 73–78.
3. F. Neese, *Wires Comput. Mol. Sci.*, 2018, **8**, e1327.
4. T. Lu and F. Chen, *J. Comput. Chem.*, 2012, **33**, 580–592.
5. W. Humphrey, A. Dalke and K. Schulten, *J. Mol. Graph.*, 1996, **14**, 33–38.
6. Z. Liu, T. Lu and Q. Chen, *Carbon*, 2020, **165**, 461–467.